Nanoscale Res Lett (2009) 4:1064–1072
DOI 10.1007/s11671-009-9359-x

NANO EXPRESS

Water-Driven Assembly of Laser Ablation-Induced Au Condensates as Mesomorphic Nano- and Micro-Tubes

Chang-Ning Huang · Shuei-Yuan Chen · Yuyuan Zheng · Pouyan Shen

Received: 22 April 2009 / Accepted: 24 May 2009 / Published online: 6 June 2009

Abstract Reddish Au condensates, predominant atom clusters and minor amount of multiply twinned particles and fcc nanoparticles with internal compressive stress, were produced by pulsed laser ablation on gold target in de-ionized water under a very high power density. Such condensates were self-assembled as lamellae and then nano- to micro-diameter tubes with multiple walls when aged at room temperature in water for up to 40 days. The nano- and micro-tubes have a lamellar- and relaxed fcc-type wall, respectively, both following partial epitaxial relationship with the co-existing multiply twinned nanoparticles. The entangled tubes, being mesomorphic with a large extent of bifurcation, flexibility, opaqueness, and surface-enhanced Raman scattering, may have potential encapsulated and catalytic/label applications in biomedical systems.

Keywords Gold · Nanocondensates · Nanotubes · Self-assembly · Water

Electronic supplementary material The online version of this article (doi:10.1007/s11671-009-9359-x) contains supplementary material, which is available to authorized users.

C.-N. Huang · Y. Zheng · P. Shen (✉)
Institute of Materials Science and Engineering, Department of Materials and Optoelectronic Science, Center for Nanoscience and Nanotechnology, National Sun Yat-sen University, Kaohsiung, Taiwan, ROC
e-mail: pshen@mail.nsysu.edu.tw

S.-Y. Chen
Department of Mechanical and Automation Engineering, I-Shou University, Kaohsiung, Taiwan, ROC

Introduction

Under ambient pressure condition, Au atoms condense in the order of increasing particle size, as structural motifs of atom clusters with planar, cage or pyramid structures [1–3], an anomalous multiply twinned particle (MTP) of decahedral (Dh) and icosahedron (Ih) types [4, 5] and a face-centered cubic (fcc) structure. On the other hand, helical gold rolling into multi-shell nanowire [6] and nanotube [7] was demonstrated via a top–down approach such as electron beam thinning.

Pulsed laser ablation (PLA) technique with a very rapid heating/cooling and hence pressure effect, as in the syntheses of dense dioxide nanocondensates with considerable internal stress [8], has been used to fabricate Au nanocondensates [9]. A high laser power density was found to cause atom clusters in addition to much larger sized MTP/fcc nanocondensates [9].

Here we used an alternative route of pulsed laser ablation in liquid (PLAL) to form more Au atom clusters for further formation of lamellae and then multiple-walled tubes (MWT) in a subsequent water-driven assembly process. This stabilizer-free approach is analogous to the fabrication of carbon onions via arc discharge in water [10], but different from surfactant/copolymers or other template-assisted assembly of Au nanoparticles in a desired manner and quantum-size-related properties for applications toward biology, catalysis, and nanotechnology [11, 12]. The self-assembled Au tube has potential biomedical applications in view of its good bending flexibility, partial epitaxial filling of MTP/fcc particles, and surface-enhanced Raman scattering (SERS) effect useful for the detection of molecules or nanoparticles adsorbed on rough metal surfaces [13, 14].

Experimental Section

PLAL Synthesis and Further Aging of Au Nanocondensates

To produce Au nanocondensates, Au (99.99% pure, 0.3 mm in thickness) foil immersed in de-ionized (DI) water within a glass beaker was subjected to energetic Nd-YAG-laser (Lotis, 1,064 nm in wavelength, beam mode: TEM00) pulse irradiation for up to 3,000 pulses inside an ablation chamber under the laser parameters compiled in Table 1. A relatively high power density of 1.4×10^{12} W/cm^2 (i.e., pulsed energy 650 mJ/pulse; pulse duration 16 ns; beam size 0.03 mm^2; fluence 2.2 kJ/cm^2; frequency 10 Hz under Q-switch mode) caused a larger yield of atom clusters as a colloidal solution. The reddish solution was then settled in capped vial for up to 40 days in desiccators or open air in order to study the influence of moisture on the assembly and migration of the resultant MWTs.

Characterization

The optical absorbance of the as-deposited nanocondensates and further developed MWTs in solution with specified dwelling times was acquired by a UV–vis spectrophotometer (U-3900H, Hitachi) operating at an instrumental resolution of 0.1 nm in the range of 300–800 nm. The powders recovered from such samples were dried for microstructure observations using optical polarized microscopy and scanning electron microscopy (SEM, JEOL JSM-6700F, 10 kV, 10 μA). The crystal structure of the MWTs was determined by X-ray diffraction (XRD, Siemens D5000, Cu Kα, 40 kV, 30 mA, at 0.05° and 3 s per step from 2θ angle for 30° up to 90°). The d-spacings measured from XRD trace were used for least-squares refinement of the lattice parameters with an error ±0.0001 nm using bulk gold reflections as a standard. Field emission transmission electron microscopy (TEM, FEI Tecnai G2 F20 at 200 kV) with selected area electron diffraction (SAED), and point-count energy dispersive X-ray (EDX) analysis at a beam size of 1 nm was used to study the composition and phases of the tubular walls. Lattice imaging coupled with two-dimensional (2-D) Fourier transform and inverse transform were used to study the rolling planes of the MWT and their partial epitaxy relationship with the associated MTP/fcc nanoparticles. Powdery sample mixed with KBr was studied by FTIR (Bruker 66v/S) for the extent of OH^- signature on MWT. As for the SERS effect, the powdery MWTs settled on a vitreous SiO_2 substrate were studied by micro-Raman in a backscattering geometry by a Jobin Yvon T64000 system working in the triple-subtractive mode.

Results

Optical Absorbance of the Condensate Solution

The colloidal Au solution as formed via PLAL is reddish under the naked eye (Fig. 1). The corresponding surface plasmon absorbance near 525 nm is similar to that of the Au nanoparticles and clusters in aqueous or solvent-protected solution [15, 16]. Room-temperature aging of the solution for up to 40 days caused progressive lowering of the absorbance peak because more opaque materials were deposited at the bottom and even along the humidified wall of the capped bottle especially when desiccated (Fig. 1).

Table 1 Laser ablation parameters and resultant phase assemblages of Au via PLAL

1,064 nm excitation	FR	QS	QS
Pulsed energy (mJ/pulse)	1,100	550	650
Pulse duration	0.24 ms	16 ns	16 ns
Beam size (mm^2)	0.03	0.03	0.03
Fluence (kJ/cm^2)	3.7	1.8	2.2
Frequency (Hz)	10	10	10
Power density (10^7 W/cm^2)	15	1.1×10^5	1.4×10^5
Ablation time (min)	15	5	5
Phases	MTP > fcc	C > MTP > fcc	C > MTP > fcc > T
Mean particle size (nm)	5	6.5	7.5
Residual stress (GPa)*	6.3	8.1	8.5

FR and *QS* denote free run and Q-switch mode, respectively. *MTP* denotes multiply twinned particle, *C* cluster, *fcc* face-centered cubic, and *T* tubes

* Based on SAED lattice parameter of the fcc/MTP nanocondensates and the Birch-Murnaghan equation of state of fcc gold with relevant bulk modulus and its pressure derivative (cf. text)

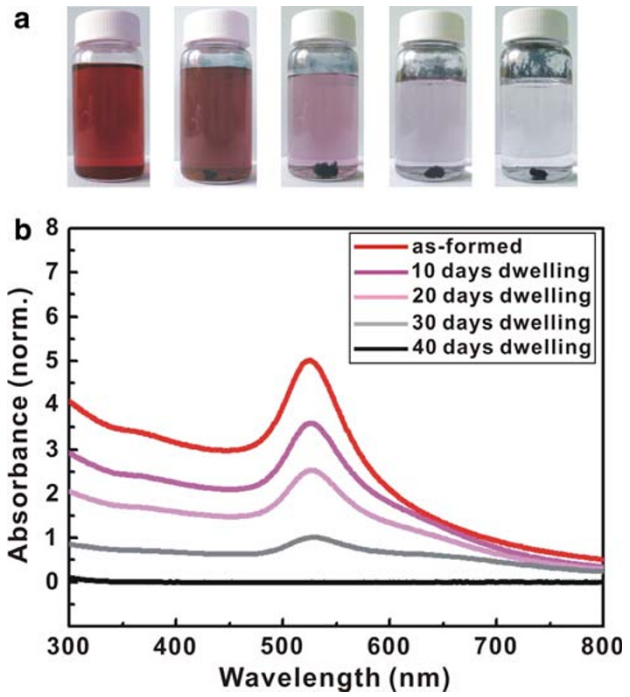

Fig. 1 Color change of reddish colloidal Au solutions. **a** Produced via PLAL followed by further aging in desiccators for up to 40 days (from *left to right*) to deposit opaque materials, i.e., lamellae and microtubes (cf. text). **b** Corresponding optical absorption spectra (from *top to bottom*) showing gradual lowering of the absorbance peak near 525 nm, in accordance with the sedimentation of lamellae and then tubular materials at the expense of atom clusters

The opaque materials are in fact mesomorphic lamellae and MWTs as indicated by the following electron microscopic observations.

Structural Development of Nanocondensates upon Aging in Water

The powdery materials retrieved from the colloidal Au solution having been processed by PLAL were agglomerated as nanoparticle chain aggregate (NCA), as shown by the TEM bright field image (BFI) in Fig. 2a. The individual atom clusters and MTP/fcc particles within the NCA were imaged (Fig. 2b, c) using the low-angle scattering halo (Fig. 2d) and the nearly superimposed strong {111}/{200} diffractions of the MTP/fcc (Fig. 2d), respectively. The diffraction intensity profile (Fig. 2e) further showed that the low-angle scattering of the atom clusters falls in the range of 1.46–1.78 Q^{-1} full width at half-height, analogous to that of the polished Beilby layers [17] or Au foil on the verge of melting [18]. EDX analysis on the nanocondensates (Fig. 2f) showed Au peaks, with the remaining peaks from the supporting carbon-coated collodion film and Cu grid. This result indicates that oxidation or contamination of the Au nanocondensates is negligible.

After aging for 10 days in water, the Au atom clusters were self-assembled as corrugated lamellae as shown by the TEM BFI in Fig. 3a. The SAED pattern (Fig. 3b) and corresponding diffraction intensity profile (Fig. 3c) showed a broad diffraction near 1.63 nm^{-1} for atom clusters, a sharp diffraction at 2.84 nm^{-1} for Au nanotubes and broad diffractions near 4.21, 4.65, 6.96, 7.96 nm^{-1} for (111), (200), (220), and (311) of MTP/fcc nanoparticles, respectively. Lattice images further indicated the lamellae are bifurcated and entangled (Fig. 3d), yet having lamellar layer nearly parallel to (200) and/or (111) of MTP (Fig. 3e, f), i.e., following partial epitaxy relationship.

The final products after aging for 40 days in water are tubular Au wires which are about 2–5 μm in width and several hundreds of micrometers in length as indicated by SEM observation (Fig. 4a). The microtubes showed extensive branches and entanglement having walls decorated with Au nanoparticles when imaged at a higher magnification (Fig. 4b). TEM further showed that the microtubes are either uncapped or capped (Fig. 4c, d) having randomly oriented fcc-type domains in the wall, and a hollow core of such tubes was manifested by a relative weak diffraction in the center of the tubes. XRD trace (Fig. 4e) and the structure refinement of the d-spacings further indicated that the fcc-type wall newly assembled from atom clusters has a rather relaxed lattice parameter ($a = 0.4075$ nm) close to the ambient value ($a = 0.4079$ nm, JCPDS file 04-0784). By contrast, there is a much smaller SAED lattice parameter (0.402 ± 0.002 nm) for the as-formed fcc nanocondensates than the relaxed fcc-type wall of the microtubes ($a = 0.408 \pm 0.002$ nm) implying a significant internal stress as discussed later.

Further TEM scrutiny revealed a typical nanotube with a varied diameter ranging from $\sim$100 nm on the one end to less than 10 nm on the other end (Fig. 5a). The BFIs magnified from the specified regions of the nanotube showed encapsulated fcc and MTP nanoparticles which have much stronger diffraction contrast than the lamellar wall (Fig. 5b, c). The identity of lamellae within the corrugated wall of the MTP/fcc encapsulated nanotube was confirmed by high-resolution TEM image (Fig. 5d) and corresponding SAED pattern (Fig. 5e) coupled with intensity profile (Fig. 5f). Point-count EDX analysis on the lamellar wall with weak Bragg diffraction contrast, i.e., immune from fcc/MTP nanoparticles, showed Au counts without appreciable oxygen and impurities.

Optical Properties and Surface-Enhanced Raman Scattering of Au Microtubes

The hollow core and optically isotropic wall of the Au microtubes were manifested by optical polarized microscopic observation under a single polarizer and crossed

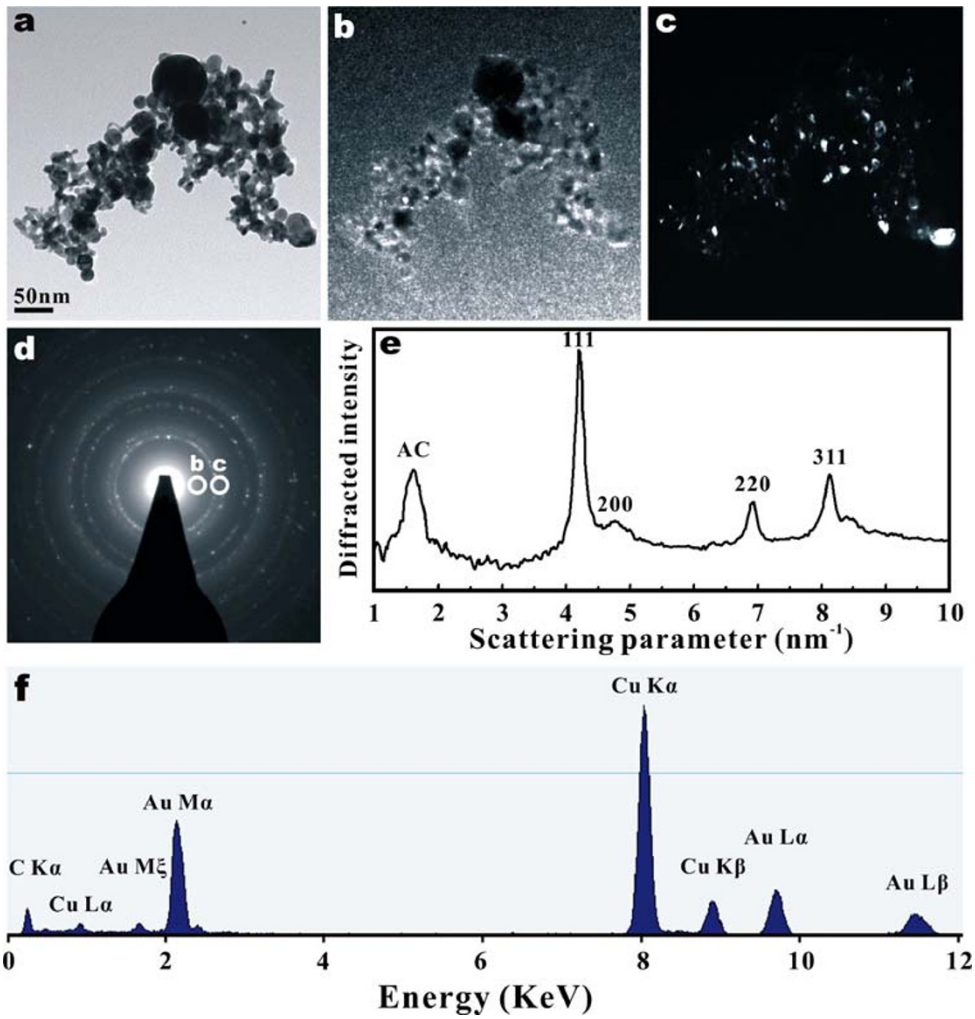

Fig. 2 TEM of Au nanocondensates produced via PLAL on Au target at 1.4×10^{12} W/cm^2. **a** BFI, **b**, **c** dark field images using low-angle scattering and nearly superimposed {111}/{200} diffractions, respectively, as circled in SAED pattern in (**d**) with corresponding intensity profiles in (**e**), to show atom clusters (denoted as *AC*) and MTP/fcc particles, respectively. **f** Point-count EDX spectrum of the Au nanocondensates showing Au counts with negligible O and impurities. The Cu count is from the sample supporting copper grid and C from carbon-coated collodion film

polarizers, respectively (not shown). The wall of such microtubes showed significant light reflection despite the dark appearance of the sediments under the naked eye. The absence of metallic luster for the microtubes can be attributed to the surface roughness and defects of the wall.

The Raman shift of the as-formed Au condensates and subsequently assembled microtubes on a substrate of vitreous silica showed a significant SERS effect (Fig. 6). The vitreous silica alone is characterized by the vibrational D_1 and D_2 Raman bands at 488 and 599 cm^{-1} (Fig. 6a), which have been assigned to small planar ring [19] and/or paracrystalline cluster interface [20]. When such a substrate was overlaid with the as-formed Au condensates (blue trace in Fig. 6b) or subsequently assembled Au microtubes (red trace in Fig. 6b), both D_1, D_2, and minor unidentified bands became one to two-orders-of magnitude higher. In both cases, the D_1 mode shift significantly because of the selection rules [21]. It should be noted that the SERS effect is more pronounced to have a higher signal to noise ratio for the assembled Au microtubes than the as-formed Au condensates. The OH^- signature of the microtubes was indicated by a typical FTIR spectrum showing a significant peak near 3,432 cm^{-1} (Fig. 6c) which can be assigned as OH stretching vibration [22].

Discussion

Comparison of Au Condensates via PLAL vs. PLA

In comparison with that fabricated by PLA [9], The present Au condensates via PLAL have much more atom clusters than MTP and fcc. This can be attributed to an order-of-magnitude higher heating-cooling rate (ca. 1×10^{10} K/s) for PLAL [23] than PLA process and hence a pressure effect to form smaller sized nanocondensates. Base on Birch–Murnaghan equation of state and relevant bulk modulus $B_0 = 166.7$ GPa as well as its pressure derivative $B_0' = 5.48$ for bulk fcc Au at zero pressure and 298 K [24, 25], the internal compressive stress of the as-formed

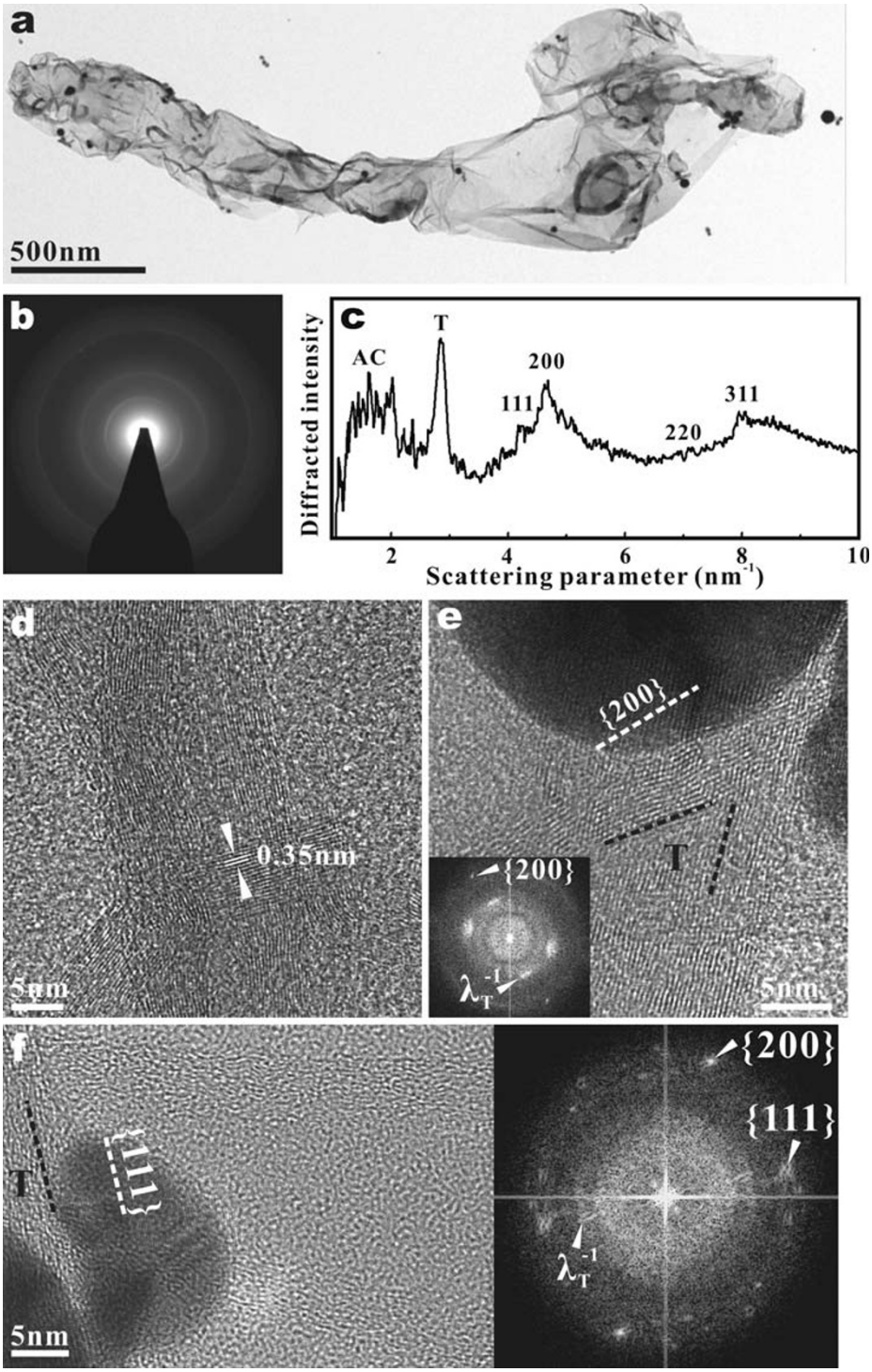

Fig. 3 TEM of corrugated lamellae derived from the condensed atom clusters in Fig. 2 by further room-temperature aging for 10 days in water. **a**, **b** BFI and SAED pattern. **c** Intensity profile across the diffraction rings in SAED pattern showing diffractions of atomic clusters (denoted as *AC*), nanotubes (denoted as *T*) and MTP/fcc nanoparticles with (hkl) specified. **d** Lattice imaging shows bifurcation/entanglement of the lamellae as well as (**e**) and (**f**) partial epitaxy nucleation of the lamellae from MTP having one of the penetrating lamellar layer sets (denoted as black *dotted lines*) nearly parallel to (200) and (111) of MTP, respectively

fcc nanocondensates was calculated to increase up to ~8 GPa with the increase of PLAL power density (Table 1).

A high quenching rate of laser-induced plasma in confining liquid was known to cause metastable phase, such as diamond, that is thermodynamically stable in high-temperature high-pressure regime [26]. The estimated compressive stress level up to ca. 8 GPa is not high enough to stabilize the high-pressure hcp phase, which typically occurs above ~240 GPa at ambient temperature [27]. The reasons to retain a high internal stress for the fcc nanocondensates may include a very high quenching rate, the capillarity force under nanosize effect, and the constraint exerted by partially epitaxial MTPs. It should be noted that

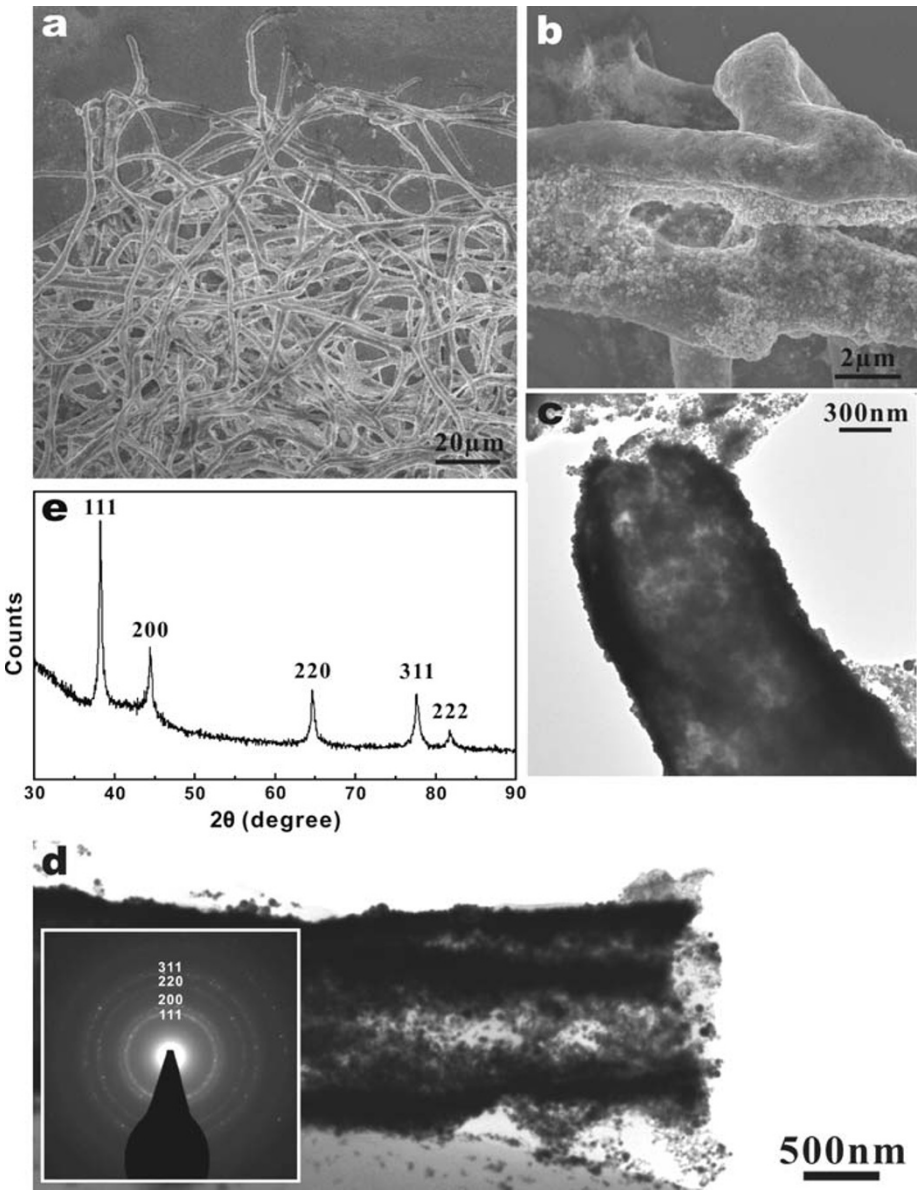

Fig. 4 Microstructures of the Au microtubes revealed by (**a**), (**b**) SEM secondary electron images at low and high magnifications, respectively; (**c**), (**d**) TEM BFI of the capped and uncapped Au microtubes, respectively, both having polycrystalline wall of fcc structure as indicated by a representative SAED pattern inset; (**e**) XRD pattern (CuKα) of the bifurcated Au microtubes with fcc-type wall. Such tubular materials were developed from the Au nanocondensates fabricated by PLAL under Q-switch mode followed by 40 days dwelling in the same aqueous solution at room temperature

the internal stress remained nearly unchanged for the fcc nanocondensates after room-temperature aging for 40 days in water (not shown). The relaxed fcc-type wall of the microtubes thus has nothing to do with such nanocondensates. Instead, they were derived from atom clusters through an intermediate lamellar phase. The driving force for the formation of such a mesomorphic phase was likely total surface reduction under the influence of water for hydrogen-bonding related coordination change of Au atoms.

Water-Driven Rolling and Transformation of Lamellae in the Absence of Surfactant

The present Au nano- and micro-tubes were able to develop from atom clusters and then lamellae for further rolling in aqueous solution without the assistance of artificial surfactant for the following reasons. The atom clusters were likely self-assembled into lamellae under the influence of hydration effect, as indicated by OH stretching mode in the FTIR spectrum (Fig. 6c), in order to reduce the exposed surface area and to modify the structure of nanoparticles as the case of other materials [28]. The mesomorphic rolling of the Au lamella was then triggered by the mismatch strain of its structure units with considerable distortion and residual stress due to a dynamic PLAL process. The lamellae could possibly be made of atom clusters in the form of trigonal planar and pentagonal pyramid with electron positive ligands that donate electron density to the relativistically contracted and stabilized Au 6s orbital, and thus enhance the aurophilic interactions [29],

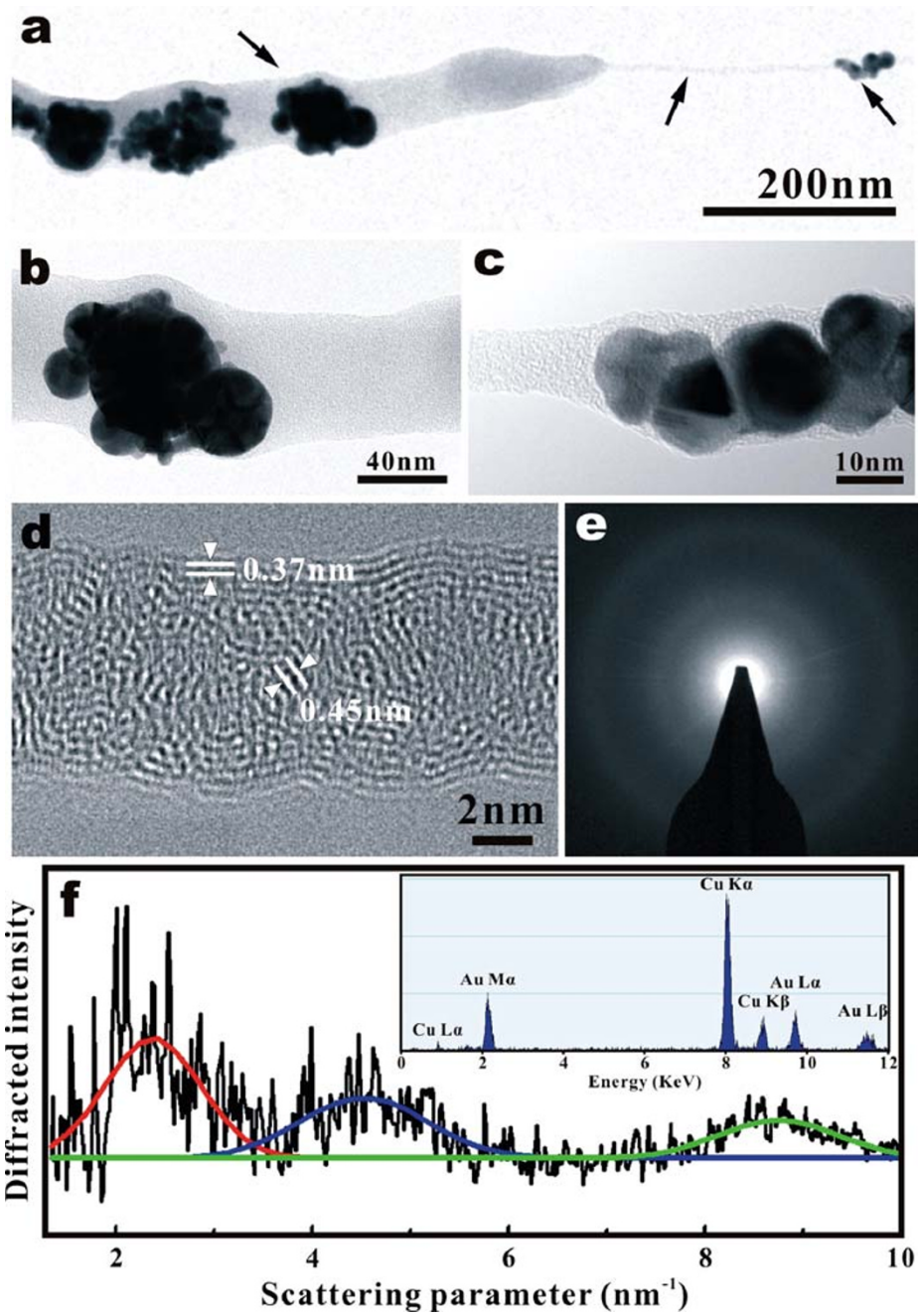

Fig. 5 Microstructures of a typical Au nanotube. (**a**) TEM BFI showing a varied diameter ranging from ~100 nm on the one end to less than 10 nm on the other end. (**b**), (**c**) BFIs magnified from regions indicated by *arrows* showing encapsulated fcc/MTP nanoparticles with strong Bragg diffraction contrast. (**d**) Lattice image taken from the bridge (*arrow*) in (**a**) showing the nanotube has four defective lamellar layers nearly edge on in the wall and a hollow core with the lamellar wall in *top view*. (**e**), (**f**) Corresponding SAED pattern and intensity profile showing strong broad diffractions with maximum intensity at 2.45, 4.58, and 8.74 cm^{-1}, i.e., plane interspacing 0.408, 0.218, and 0.114 nm, for the tubular lamella wall, nearly superimposed (111)/(200) and (311)-motif of the encapsulated MTP/fcc, respectively. The MTP/fcc encapsulated tubes are Au without appreciable oxygen and impurities according to EDX spectrum inset. The same specimen as in Fig. 4

or alternatively distorted hexagon as a precursor of fcc structure motif. In any case, the anisotropic strain among the randomly distributed atom clusters with directional ligands throughout the network would cause the lamella to roll up in order to minimize the dangling bonds analogous to the case of carbon nanotubes [30]. Such energetic favorable rolling of the structural units is also adopted by viruses, Buckminster fullerene [30], and chrysotile, a well-known fiber tubular mineral having is curvature determined by the degree of mismatch between the cations occupying the tetrahedral and octahedral layers [31].

It should be noted that the lamellar wall turned into fcc-type structure when the nanotubes were coarsened up to microns in diameter. This indicates that size dependent chemical free energy is of concern to form a more stable close packed structure for the tube wall. A partial epitaxial nucleation route by (111) or $(200)_{MTP}$//lamella layer may also lower the activation energy for the lamellar wall to change into fcc structure.

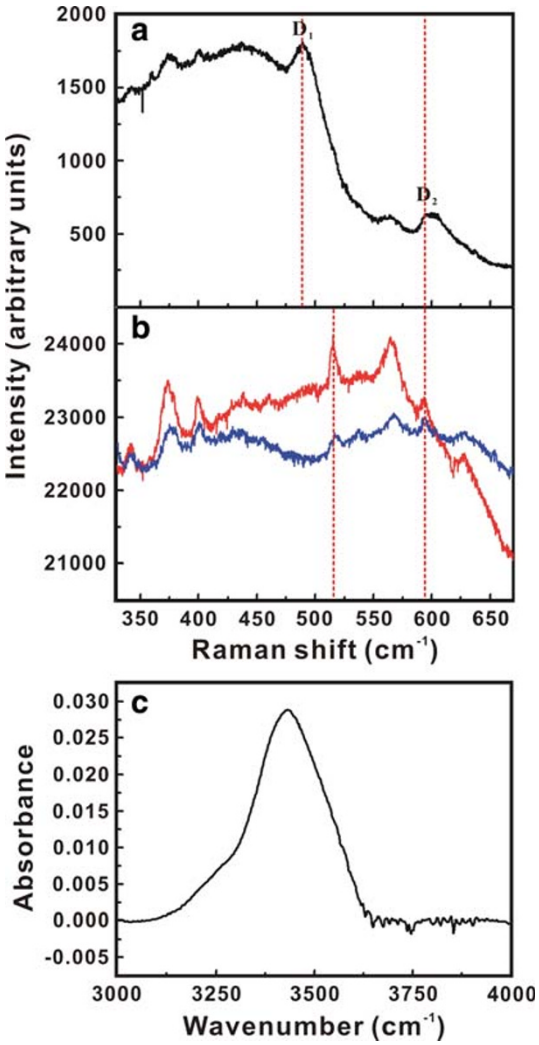

Fig. 6 Vibrational spectrum of the deposit of Au microtubes on vitrous silica. **a**, **b** Raman shift of vitreous silica without and with the deposit of the as-formed Au condensates (*blue trace*) and subsequently assembled Au microtubes (*red trace*, the same material as in Fig. 4), respectively, showing surface-enhanced Raman scattering of D_1 and D_2 modes (cf. text), and minor unidentified bands, **c** FTIR spectrum showing OH^- stretching vibration near 3432 cm^{-1} [22]

Phase Behavior of Hydrophilic Au Microtubes

The mesomorphic Au microtubes were able to migrate along the humidified wall of the capped bottle especially when desiccated. This indicates that the outer surface of the Au microtube is hydrophilic. This hydration nature is in drastic contrast with the case of carbon nano-onions floating on the water surface or falling to the bottom of the container [10], and carbon nanotubes by PECVD or pyrolysis in the absence of surfactant [32, 33]. Still, it is not clear if the Au nanotube has hydrophobic channel for tight hydrogen-bonding network facilitated conduction of water analogous to the case of carbon nanotube with the channel occupancy and conductivity tunable by the change in the local polarity and solvent condition [34].

Concluding Remarks

As a final remark, PLAL is an effective process to fabricate atom clusters for further water-driven assembly of lamellae which rolled into tubular materials under the influence of atom clusters misfit strain and hydration effect. The resultant Au microtubes with a large extent of bifurcation, inner wall exposure, and flexibility as well as SERS effect may have potential encapsulated and catalytic/label applications in biomedical systems. Further study is required to clarify if the PLAL synthesis of semiconducting nano- and micron-tubes can be extended to other noble metals.

Acknowledgments We thank Dr. R.H. Hsu for helpful discussion on UV–visible spectrum and an anonymous referee for constructive comments. This work was supported by Center for Nanoscience and Nanotechnology at NSYSU and National Science Council, Taiwan, ROC.

References

1. M.P. Johansson, D. Sundholm, J. Vaara, Angew. Chem. Int. Ed. Engl. **43**, 2678 (2004). doi:10.1002/anie.200453986
2. X. Gu, M. Ji, S.H. Wei, X.G. Gong, Phys. Rev. B **70**, 205401 (2004). doi:10.1103/PhysRevB.70.205401
3. S. Bulusu, X. Li, L.S. Wang, X.C. Zeng, Proc. Natl. Acad. Sci. USA **103**, 8326 (2006). doi:10.1073/pnas.0600637103
4. S. Iijima, T. Ichihashi, Phys. Rev. Lett. **56**, 616 (1986). doi:10.1103/PhysRevLett.56.616
5. P.A. Buffat, M. Flüeli, R. Spycher, P. Stadelmann, J.P. Borel, Faraday Discuss **92**, 173 (1991). doi:10.1039/fd9919200173
6. Y. Kondo, K. Takayanagi, Science **289**, 606 (2000). doi:10.1126/science.289.5479.606
7. Y. Oshima, A. Onga, K. Takayanagi, Phys. Rev. Lett. **91**, 205503 (2003). doi:10.1103/PhysRevLett.91.205503
8. S.Y. Chen, P. Shen, Phys. Rev. Lett. **89**, 096106 (2002). doi:10.1103/PhysRevLett.89.096106
9. C.N. Huang, S.Y. Chen, Y. Zheng, P. Shen, J. Phys. Chem. C **112**, 14965 (2008). doi:10.1021/jp805254h
10. N. Sano, H. Wang, M. Chhowalla, I. Alexandrou, G.A.J. Amaratunga, Nature **414**, 506 (2001). doi:10.1038/35107141
11. M. Kim, K. Sohn, H.B. Na, T. Hyeon, Nano. Lett. **2**, 1383 (2002). doi:10.1021/nl025820j
12. M.C. Daniel, D. Astruc, Chem. Rev. **104**, 293 (2004). doi:10.1021/cr030698+
13. P.C. Lee, D. Meisel, J. Phys. Chem. **86**, 3391 (1982). doi:10.1021/j100214a025
14. S. Nie, S.R. Emory, Science **275**, 1102 (1997). doi:10.1126/science.275.5303.1102
15. S. Link, M.A. El-Sayed, J. Phys. Chem. B **103**, 4212 (1999). doi:10.1021/jp984796o
16. A.C. Templeton, J.J. Pietron, R.W. Murray, P. Mulvaney, J. Phys. Chem. B **104**, 564 (2000). doi:10.1021/jp991889c
17. K. Nonaka, K. Kohra, J. Phys. Soc. Jpn. **9**, 512 (1954). doi:10.1143/JPSJ.9.512

18. T. Suzuki, J. Phys. Soc. Jpn. **10**, 1026 (1950). doi:10.1143/JPSJ.10.1026
19. F.L. Galeener, J. Non-Cryst. Solids **49**, 53 (1982). doi:10.1016/0022-3093(82)90108-9
20. J.C. Phillips, J. Non-Cryst. Solids **63**, 347 (1984). doi:10.1016/0022-3093(84)90102-9
21. M. Moskovits, J.S. Suh, J. Phys. Chem. **88**, 5526 (1984). doi:10.1021/j150667a013
22. A. Putnis, B. Winkler, L. Fernandez-Diaz, Mineral. Mag. **54**, 123 (1990). doi:10.1180/minmag.1990.054.374.14
23. K. Saito, K. Takatani, T. Sakka, Y.H. Ogata, Appl. Surf. Sci. **197–198**, 56 (2002). doi:10.1016/S0169-4332(02)00303-3
24. D.L. Heinz, R. Jeanloz, J. Appl. Phys. **55**, 885 (1984). doi:10.1063/1.333139
25. R. Ahuja, S. Rekhi, B. Johansson, Phys. Rev. B **63**, 212101 (2001). doi:10.1103/PhysRevB.63.212101
26. G.W. Yang, Prog. Mater. Sci. **52**, 648 (2007). doi:10.1016/j.pmatsci.2006.10.016
27. L. Dubrovinsky, N. Dubrovinskaia, W.A. Crichton, A.S. Mikhaylushkin, S.L. Simak, I.A. Abrikosov, J.S. de Almeida, R. Ahuja, W. Luo, B. Johansson, Phys. Rev. Lett. **98**, 045503 (2007). doi:10.1103/PhysRevLett.98.045503
28. H. Zhang, B. Gilbert, F. Huang, J.F. Banfield, Nature **424**, 1025 (2003). doi:10.1038/nature01845
29. P. Schwerdtfeger, Angew. Chem. Int. Ed. Engl. **42**, 1892 (2003). doi:10.1002/anie.200201610
30. P.J.F. Harris, *Carbon nanotubes and related structures: new materials for the twenty-first century* (Cambridge University Press, New York, 1999)
31. A. Putnis, *Introduction to mineral science* (Cambridge University Press, Cambridge, 1992)
32. P. Joseph, C. Cottin-Bizonne, J.M. Benoit, C. Ybert, C. Journet, P. Tabeling, L. Bocquet, Phys. Rev. Lett. **97**, 156104 (2006). doi:10.1103/PhysRevLett.97.156104
33. H. Li, X. Wang, Y. Song, Y. Liu, Q. Li, L. Jiang, D. Zhu, Angew. Chem. Int. Ed **40**, 1743 (2001). doi:10.1002/1521-3773(20010504)40:9<1743::AID-ANIE17430>3.0.CO;2-#
34. G. Hummer, J.C. Rasaiah, J.P. Noworyta, Nature **414**, 188 (2001). doi:10.1038/35102535